International Journal of Thin Films Science and Technology

http://dx.doi.org/10.18576/ijtfst/120307

Roles of Oxygen Vacancies and Excess Electron Localization on Ceria Surfaces: First Principles Study

Nabil Al Aqtash[1,], Anas Y. Al-Reyahi[1], Said M. Al Azar[2], Ahmad Mufleh[3], Saber S. Essaoud[4], and Khadidja Berarma[5].*

[1] Department of Physics, Faculty of Science, The Hashemite University, P. O. Box 330127, Zarqa 13133, Jordan
[2] Department of Physics, Faculty of Science, Zarqa University, Zarqa 13132, Jordan
[3] Preparatory Deanship, Prince Sattam Bin Abdulaziz University ,Al-Kharj, Saudi Arabia
[4] Laboratoire de Physique des Particules et Physique Statistique, Ecole Normale Supérieure-Kouba, BP 92, Vieux-Kouba, 16050 Algiers, Algeria
[5] Laboratory of Inorganic Materials, Department of Chemistry, University of M'sila, 28000 M'sila, Algeria

Received: 16 May 2023, Revised: 29 Aug. 2023, Accepted: 31 Aug. 2023
Published online: 1 Sep. 2023.

Abstract: In this study, we investigate the (111), (110) and (100) surfaces of reduced ceria (CeO2) using density functional theory (DFT) within DFT+U. We examine the process by which oxygen vacancy sites form on CeO2 (111), (110), and (100) surfaces as well as the stability of these sites close to the ceria surface regions. Our calculations demonstrate that electron localizations of the reduced CeO2 on each of these three surface terminations are caused by oxygen vacancies, both surface and subsurface, which results in the emergence of Ce^{3+} sites. The oxygen vacancy at the surface and subsurface of CeO2 (111) surfaces results in the formation of Ce^{3+} at the vacancy's next-closest neighbor. Ce^{3+} is formed at the sites closest to the oxygen vacancy sites on CeO_2 (100) and CeO_2 (110) surfaces. The calculated total density of states (TDOS) of the reduced surfaces displays that the Ce 4*f* states are partially occupied and appeared in a new state near the band gap compared to that for the unreduced ceria surfaces. The existence of these new states was found to have a large effect on the nature of ceria. In (111) ceria surface, the material remains semiconductor with a smaller band gap. However, (110) and (100) ceria surfaces become semi-metallic due to the crossing of a new state of the fermi level that converts ceria to become semi-metallic material. Therefore, the conductivity and chemical properties of ceria are expected to be modified by the creation of oxygen vacancy. The reduced ceria expects to catalyze the dissociation of molecules on its surface. The dissociation is assisted by the oxidation of Ce^{3+} that is generated on reduced ceria surfaces.

Keywords: Ceria; DFT+U; oxygen vacancy; electron localization.

1. Introduction

Ceria (CeO_2) is a well-known catalyst component for petroleum cracking, chemo-selective organic reactions, and automobile exhaust converters due to its exceptional redox and oxygen storage capabilities [1–5]. CeO_2 can be chemically resilient and goes through repeatable Ce^{4+}/Ce^{3+} redox cycles depending on the operating conditions [6,7]. Ceria has a quick reduction rate, but it typically has a slow oxidation rate [8]. The potential for CeO_2 to be reduced and oxidized has thus been the subject of numerous research investigations. Based on these investigations, it is concluded that oxygen diffusion, which can be observed in the form, size, and concentration of oxygen vacancy sites, is the essential rate-controlling process. For instance, using high-resolution scanning tunneling microscopy (STM), Esch et al. [9] observed the oxygen vacancy defect (OVD), including those small clusters of linear surface oxygen vacancy sites on CeO_2 (111). The electrons that the released oxygen has left behind concentrate on cerium ions [9]. Since then, various studies have used STM and dynamic force microscopy with atomic resolution [10, 11].

On the reduced CeO_2 (111) surfaces, the surface and subsurface oxygen vacancies have been investigated using density functional theory (DFT) [11–14]. There have been reports of vacancy-induced lattice relaxation, excess electron localization, and local ordering surface defects. Recently, Wu and Gong [15] asserted that those reported defects were actually hydroxyl-vacancy combined species rather than just oxygen vacancies or other impurities as suggested by Kullgren et al [16] based on their DFT calculation results. Therefore, determining the precise roles of oxygen vacancies is essential for understanding CeO_2's catalytic activity. However, there are still unresolved theoretical explanations for how these advantageous defects form and how they affect the reducibility and activity of nanosized ceria at the atomic level.

In this work, we investigate the process by which oxygen vacancy sites form on CeO_2(111), CeO_2(110), and CeO_2(100) surfaces as well as the stability of these sites close to the ceria surface regions. Although numerous common low-index surfaces were actively utilized in catalysis experiments with nanoscale materials. Therefore, using density functional theory (DFT) within LSDA+U, we

*Corresponding author E-mail: nabild@hu.edu.jo

conducted a comparative study of the reduced CeO_2 of the three low-index surfaces with a single oxygen vacancy site. We discussed the key conclusions and outcomes of our calculations, including the reconstruction of surfaces, the energies involved in forming the oxygen vacancies, and atomic charges on the surfaces.

2. Theoretical Methods

CeO2 belongs to the Fm-3m (225) space group. Eight O atoms and four Ce atoms make up its unit cell. Projector augmented wave (PAW) calculations with density functional theory (DFT) plane waves as implemented in the Vienna ab initio simulation package (VASP) package [17,18] is used for modeling ceria. The calculation made use of the local spin density approximation (LSDA+U or LDA+U) method with Ceperly-Alder as the exchange-correlation functional. For better convergence of the system, where energies converged until 10^{-6} eV, the cutoff energy of 400 eV was considered. We used the on-site electron repulsion U value that is most appropriate for the analysis of CeO_2. The LDA+U method successfully reproduced the experimental lattice constant, *a* (5.406 - 5.410 Å) at room temperature [19,20]. The calculated equilibrium lattice parameter (5.402 Å) is close to the experimental value [21,22] at U equal 5 eV. Lattice parameters were larger by 0.05 Å using a different strategy based on the generalized gradient approximation method (GGA+U). This was in good agreement with what was previously reported using GGA+U, but it overestimated the lattice parameter significantly compared to the experimental as well as LDA+U calculations[23,24].

Ceria surfaces with slab geometries were built using the computed lattice constant for the equilibrium bulk geometry. The separation of these slabs from their periodic images required the introduction of a vacuum of at least 15 Å normal to the surface. Table 1 contains supercell structures parameters, such as number of the unit cells, *k*-points grid, and lattice parameters.

Table 1: Specifications of the supercell structures that were used in the calculations of the surface characteristics of the three CeO2 surface terminations (111), (110), and (100).

Ceria surface	Surface unit cell	No. of *k* points	*a* (Å)	*b* (Å)	No. of atoms
(111)	3x3	2x2x1	11.47	11.47	135
(110)	3x3	2x2x1	11.47	16.23	162
(100)	2x2	5x5x1	7.65	7.65	66

3. Results and Discussion

The potential catalytic activity of the surface can be determined by examining the characteristics of oxygen-deficient surfaces. All three terminations are typically present in catalytically active nanoparticles, such as (111), (110), and (100) [9,10,25], so it is important to investigate all three of the observed terminations with a focus on the energetics and local electronic states on the surface.

Experimentally, oxygen vacancies have been found in nanostructured ceria [9,10,25]. Typically, it is challenging to produce stoichiometric CeO_2 in the Ce^{4+} oxidation state without creating vacancies, which requires reducing the material to CeO_{2-x}, where x is the oxygen concentration, as in the following reaction: $CeO_2 \leftrightarrow CeO_{2-x} + \frac{x}{2} O_2$. At x = ½, the reduction forms Ce(III) stoichiometric oxide (Ce_2O_3). Most prepared samples have x between the experimental limiting values of 0 and 0.5. The experimentally determined thermodynamic reduction energy of CeO_2 to Ce_2O_3 was found to be 3.75 eV/Ce_2O_3, which is a relatively high value given the strong covalent/ionic bonding and a consequently high melting point of Ce_2O_3 at 2670 K. However, oxygen vacancy sites are abundantly found at and near the surface of CeO_2 in experimental studies, reflecting the high catalytic activity of reduced ceria [26-29].

Calculated formation energy of oxygen for each surface as the following: $E_{va} = E_{CeO_{2-x}} + \frac{1}{2} E_{O2} - E_{CeO_2}$, where $E_{CeO_{2-x}}$ and E_{CeO_2} are the total energies of the CeO_2 slab with and without an O vacancy, respectively.

3.1 Reduced (111) CeO_2 Surface

As depicted in Figure 1, we methodically investigated various potential oxygen vacancies on the surface and subsurface layers of (111) CeO2. We were able to localize two electrons at Ce atoms close to the vacancy where the oxidation states changed from Ce^{4+} to Ce^{3+} by simply removing one oxygen atom. Ce^{3+} was discovered in several places close to the opening. For each of the cases that we looked at, we calculated the energy required to form an oxygen vacancy at the surface and below. Table 2 (with notations that match those in Figure 1) presents the DFT calculation results for the (111) surface. The locations of the Ce^{3+} charges are denoted by numbers in the second parenthesis. Ce^{3+} can be located in a number of places, including the oxygen vacancy site's nearest neighbor (N), next-nearest neighbor (NN), and even next-next neighbor (NNN). When it comes to localization, many earlier studies suggested that the subsurface oxygen vacancies are the most stable configurations according to GGA+U calculations [11,12,30-33].

The two most stable structures with a surface oxygen vacancy are NN-NN(2,8) and N-NN(4,7) (see Table 2), with respective formation energies of 3.021 and 3.018 eV. We find that Ce^{3+} tends to localize at the next nearest neighbor rather than the vacancy. Additionally, there are two configurations with subsurface oxygen vacancies, designated as N-NN(1, 7) and N-NN(5, 7) and having respective formation energies of 2.977 and 3.005 eV. Due to their similar vacancy formation energies, the surface oxygen vacancies NN-NN(2,8) and N-NN(4,7) can be regarded as degenerate or representative of all stable structures. Additionally, Table 2's formation energy values show that

OVDs preferentially form beneath the surface of the (111) surface by a difference in energy of 0.04 eV, which is consistent with earlier GGA+U results [33].

According to the scanning tunneling microscopy result of the similar vacancy concentration between these configurations [9], the most stable structures have energetic similarities to the surface and subsurface oxygen vacancies. The most stable NN-NN and N-NN configurations are also in agreement with the discovery that there can only be one extra electron localized at the Ce atom that is closest to the empty oxygen atom [11]. Recent research has revealed that the energy barrier for the electron transfer process between adjacent Ce^{3+} and Ce^{4+} centers in bulk ceria is as low as 0.4 eV, providing additional evidence for CeO_2's enhanced electron conductivity or reducibility compared to stoichiometric crystal [34]. Despite the greater elastic strain, even subsurface Ce3+ production is possible [35]. For instance, it has been discovered that subsurface Ce^{3+}, which is also the fifth subsurface atomic layer, is stable on a stepped CeO_2 surface [36]. Three locally stable structures were discovered as subsurface NN-NN(7,17), N-NN(3,14), and N-NN(5,11), with formation energies of 3.18, 3.22, and 3.27 eV, respectively. Here, we also considered Ce^{3+} for oxygen vacancy on the subsurface. As a result, the reduced CeO_2 (111) surface produces a lot of Ce^{3+} sites that are not always close to the vacancy sites, creating an "isolated" Ce^{3+} that can help with catalytic reactions that involve electron transfer.

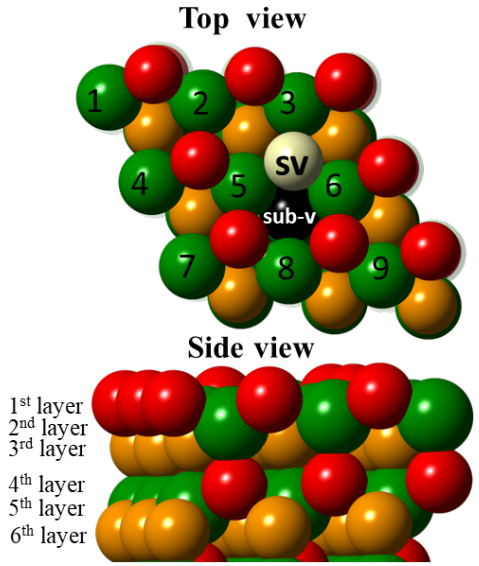

Fig. 1: Schematic of the CeO_2 (111) model surfaces (3x3 supercell): Ce atoms in the 2nd layer are numbered from 1 to 9 in order to discuss the location of Ce^{3+} sites. Atoms are colored as follows - red: oxygen in the surface layer; light brown: oxygen in the subsurface layer; green: cerium. Ce^{3+} sites are colored blue and surface vacancies (SV) and subsurface vacancies (sub-V) are colored white and black, respectively.

Table 2: Oxygen vacancy formation energy at (111) CeO_2 surface. Numbers in the second parenthesis indicate the locations of Ce^{3+} charges. Numbers 10-18 indicate the Ce atoms in the 5th layer, which are the same order of Ce atoms 1 to 9.

Ceria surface	Configuration	E_{vf} (ev)	Ce^{3+} charge localization
Bulk	O-vacancy	5.100	
(111) 3x3	Surface O-vacancy	3.021	NN-NN(2,8)
		3.018	N-N(4,7)
		3.150	N-NN(4, 8)
		3.069	N-NN(2,5)
		3.185	NN-NNN(6,9)
		3.360	NNN-NNN(1,6)
		3.044	N-N-N(4,5,7)
(111) 3x3	Subsurface O-vacancy	2.977	N-NN(1,7)
		3.005	N-NN(5,7)
		3.090	N-NN(3,4)
		3.294	N-N(4,5)
		3.225	N-NN(3,14)
		3.076	N-NN(5,11)
		3.510	N-NN(2,7)
		3.532	N-N-N(2,4,5)

The removal of an oxygen atom causes the formation of an oxygen vacancy. Ce^{4+} to Ce^{3+} transition is caused by the formation of two "unpaired" electrons after O^{2-} removal that are localized at the cerium atoms close to the vacancy. The 3-fold symmetry of the (111) surface is broken when a vacancy is introduced into the surface. Numerous Ce^{3+} sites are produced on the reduced CeO2 (111) surface, and these sites are not always located near the vacancy sites. This isolated Ce^{3+} can help with catalytic reactions that involve electron transfer. Bader charge analyses were also performed to show the charge transfer and formation of Ce^{3+} at the CeO_2 surfaces in cases of oxygen vacancy at the surface and at the subsurface. The values of induced charge (difference in charges between the reduced and unreduced surface) of Ce^{3+} atoms in reduced (111) CeO_2 surface are shown in Figure 2.

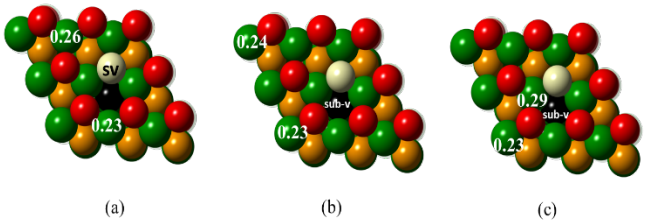

Fig. 2: Induced charges (difference in charges between the reduced and unreduced surface) of Ce^{3+} atoms in reduced (111) CeO_2 surface. (a) surface oxygen vacancy with NN-NN(2,8) Ce^{3+} case, (b) subsurface oxygen vacancy with N-

NN(1,7) Ce^{3+}case, and (c) subsurface oxygen vacancy with N-NN(5,7) Ce^{3+} case. The locations of Ce atoms on the surface as indicated in Figure 1.

The presence of an oxygen vacancy on (111) CeO_2 surface, generates two Ce^{3+} on the surface and this affects the bond between atoms due to the change in the charge distribution between the atoms, especially bonds related to Ce^{+3} atoms. The average Ce-O bond lengths in different layers of unreduced CeO_2(111) surface is between 2.33 and 2.34 Å.

As shown in Table 3, the average bond length of Ce^{3+}-O in the third layer is nearly 2.49 Å, while the average bond length of Ce^{3+}-O in the first layer is nearly 2.47 Å in the case of reduced CeO2(111) surface with surface oxygen vacancy. The values in Table 3 show that the Ce-O bond length increased from 0.13 to 0.17 Å. In both layers, the Coulomb repulsion forces between the charges on the O^{2-} atom and the Ce^{3+} cause Ce^{3+} to move farther away from the vacancy site.

Table 3: The average bond length of Ce^{3+}-O in reduced (111) CeO_2 surface. surface oxygen vacancy with NN-NN(2,8) Ce^{3+} case and subsurface oxygen vacancy with N-NN(1,7) Ce^{3+} case.

Bond length between atoms	**Average bond length in reduced surface**
surface oxygen vacancy with NN-NN(2,8) Ce^{3+}	
Ce(site 2)- O in $1^{st} layer$	2.46 Å
Ce(site 2)- O in $3^{rd} layer$	2.5 Å
Ce(site 8)- O in $1^{st} layer$	2.48 Å
Ce(site 8)- O in $3^{rd} layer$	2.47 Å
subsurface oxygen vacancy with N-NN(1,7) Ce^{3+}	
Ce(site 1)- O in 1^{st} layer	2.58 Å
Ce(site 1)-O in 2^{nd} layer	2.45 Å
Ce(site 7)- O in 1^{st} layer	2.5 Å
Ce(site 7)- O in 2^{nd} layer	2.43 Å

Additionally, as shown in Table 3, the average length bond of Ce^{3+}-O in the first layer increases from 2.33 to nearly 2.54 Å, and the average length bond of Ce^{3+}-O in the third layer increases from 2.34 to nearly 2.44 Å in the case of oxygen subsurface vacancy on (111) CeO2 surface. The Coulomb repulsion forces between Ce^{3+} and O^{2-} atom cause Ce^{3+} to move farther away from the vacancy site, much like the surface vacancy.

3.2 Reduced (110) CeO2 Surface

As depicted in Figure 3, we take into account surface and subsurface oxygen vacancy sites at (110) CeO_2 surface. Because only two Ce sites at the surface are bonding to the absent O^{2-}, the oxygen vacancy in CeO_2 (110) surface does not break symmetry like the oxygen vacancy in (111) surface. So, when an oxygen vacancy occurs, two Ce^{3+} sites are created close to the vacancy site (see Figure 3), and the surface Ce-O bonds are reduced from 2.34 Å to almost 2.27 Å. These Ce^{3+} sites are closest to the oxygen vacancy site if it is in the top surface layer. If the oxygen vacancy is formed in the subsurface layer, the Ce^{3+} sites are formed in the surface layer (closest to the vacancy site) but not at the Ce in the subsurface layer. The second Ce^{3+} is formed in the 3rd Ce layer from the top. In the subsurface layer, the structural reconstruction also results in elongated Ce-O bonds (from 2.33 to 2.5).

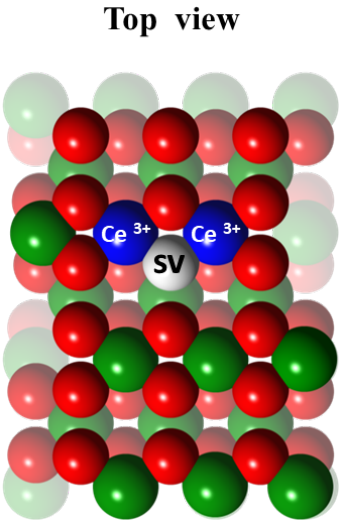

Fig. 3: Schematic of the CeO_2 (110) model surface (3x3 supercell) containing oxygen vacanvy. Atoms are colored as follows - red: oxygen in the surface layer; light brown: oxygen in the subsurface layer; green: cerium; Ce^{3+} sites are colored blue and surface vacancies (SV) and subsurface vacancies (sub-V) are colored white and black, respectively.

We determined the energy required to form oxygen vacancies at the reduced (110) CeO_2 surface and subsurface. With Ce^{3+} localized at sites (4,5) and (5,23), the formation energy for the surface oxygen vacancy is 2.5 eV, and the formation energy for the subsurface oxygen vacancy is 3.47 eV. Given that the energy required to form a surface vacancy is 1 eV less than that required to form a subsurface vacancy, we can conclude that the surface oxygen vacancy is more likely to form than the subsurface vacancy. Additionally, the reduced (110) CeO_2 surface has a surface oxygen vacancy formation energy that is about 0.5 eV lower than that of the reduced (111) CeO_2 surface, suggesting that the reduced (110) surface may be more active for surface reactions than the (111) surface. Furthermore, Bader charge analyses confirm the locations of Ce^{3+} atoms at the reduced (110) CeO_2 surface in cases of oxygen vacancy at the surface and at the subsurface. In the case of the surface oxygen vacancy, the Ce^{+3} atoms at (4,5) sites have induced chargers of 0.27 and 0.28 *e* respectively, while the Ce^{+3} atoms at (5,23) sites for the subsurface oxygen vacancy case have induced chargers of 0.23 and 0.27 *e* respectively.

3.3 Reduced (100) CeO2 Surface

Specific consideration is needed when calculating the formation energies of the (100) surface. The straightforward cleavage of (100) surface forms a polar surface. These surfaces are reconstructed to remove the electrostatic penalty of surface polarity. Predictably, about half of the oxygen

sites are removed from the unreduced surface to eliminate the polarity issue and initiate “polarity oxygen vacancies” (sites of the removed oxygen). We looked at four different surface reconstruction configurations, designated as A0, B0, C0, and D0 in Figure 4 [26]. The geometries of these surfaces are very dissimilar. In particular, the top layer of A0 has two Ce atoms per unit cell, compared to B0's four oxygen atoms and D0's two oxygen atoms. In contrast to the bulk structure, the two-layer reconstruction of C0 forms pyramids with Ce as the vertex and 6 oxygen atoms as the next layer, with two additional oxygen atoms missing from the second subsurface layer. As shown in Table 4, we determine that configurations B0 and C0 are almost degenerate in terms of formation energy. Both structures have "polarity oxygen vacancies" that may be involved in the catalytic processes because they reconstruct to have roughly half of the oxygen sites from the ideal cleavage surface removed.

Table 4: Surface formation energy densities of CeO_2 (100) surfaces.

Ceria surface		**LDA+U (eV/Å²)**	**GGA-PBE +U (eV/Å²)**
(100) (2x2)	A0	0.142	0.113
	B0	0.126	0.091
	C0	0.125	0.093
	D0	0.133	0.100

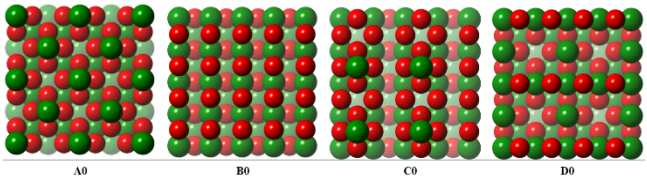

Fig. 4: Atomistic structure of four possible non-polar terminations of CeO_2 (100) surface. (red: oxygen; green: cerium). The depth fading differentiates Ce atoms in various layers.

Due to the polar nature of the cleavage surface, reconstruction usually occurs on CeO_2 surfaces. We concentrate on the development of oxygen vacancy sites on the C0 surface, which has the lowest formation energy, as shown in Table 4. At this surface, various oxygen vacancy sites were formed. The oxygen vacancy at the CeO_2 (100) C0 surface can be found in sites 1 through 3, as shown in Figure 5 (vacancy is shown in site "1," which has the lowest formation energy). The calculated oxygen vacancy formation energy for the vacancy at site “1” is 1.690 eV and for sites “2” and “3” are 3.36 eV. When a surface oxygen atom is removed from (site 1) with the lowest coordination, the vacancy formation energy is lowest; however, in the case of the two-layer pyramid, removing oxygen from (site 2) requires more energy. Because the surface symmetry is already twofold and charges tend to localize on the two Ce sites closest to the oxygen vacancy sites, we find that the formation of two Ce^{3+} sites always occur concurrently with the formation of oxygen vacancies. In every case taken into consideration, Ce^{3+} sites are located closest to the oxygen vacancy site (the location of Ce^{3+} is shown in Figure 5). Additionally, the topmost Ce site in the C0 structure is also a Ce^{3+} site.

Two Ce^{3} sites are created close to the oxygen surface vacancy (site1) on the surface of CeO_2 (100). In the case of a reduced (100) surface, the length of the Ce-O bonds increases due to the formation of Ce^{3}, whereas the length of the Ce^{3+}-O bonds increases by 0.12 Å due to the coulomb repulsion forces pushing the oxygen atom relative to the bond length of the same atoms in the case of a reduced (100) CeO_2 surface. The topmost Ce site (on the top of the pyramid) in the C0 structure produces Ce^{3} due to the presence of an oxygen surface vacancy (site2) on (100) CeO_2 surface. Due to the oxygen atom being pushed by coulomb repulsion forces away from the vacancy site, the Ce^{3+}-O bonds length increased by 0.03 Å in comparison to the unreduced (100) CeO_2 surface.

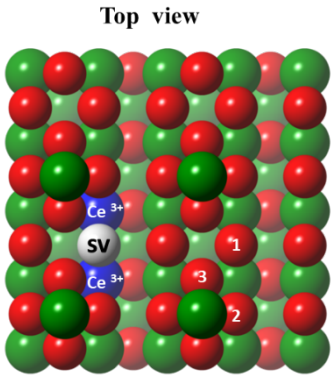

Fig. 5: Schematic of the CeO_2 (100) model surfaces (4x4 supercell): the oxygen vacancy can be located at Sites 1 through 3 (vacancy showed at the Site “1” has the lowest formation energy).

Atoms are colored as follows - red: oxygen; green: cerium; Ce^{3+} sites are colored blue and surface vacancies (SV) are colored white.

To confirm the locations of Ce^{3+} atoms at the reduced (110) CeO_2 surface in cases of oxygen vacancy at site 1 and at site2, Bader charge analyses were performed. The induced charges on Ce^{3+} atoms are 0.27 and 0.26 *e* respectively when the oxygen vacancy on site 1, while the induced charges on Ce^{3+} atoms are 0.27 and 0.26 *e* respectively when the vacancy on site 2, sites indicated in Figure 5.

In terms of formation energies, the preferential oxygen vacancy formation of the surfaces (100), (111), and (110) is discussed. The energies required to form oxygen vacancies close to the surface are much lower than the 5.1 eV reported for the bulk [23,30,31]. On the surface of (111), the formation energy of the oxygen vacancy is approximately 3 eV, whereas site 1 on the surface of (100) is 1.69 eV. When the vacancy forms on the surface of (111), three Ce-O bonds are "broken," whereas only two bonds are "broken" when the vacancy forms on the surface of (100).

3.4 Density of states

The total density of states (TDOS) is basically the number of states at a particular energy level that electrons are allowed to occupy. TDOS calculations allow us to determine the general distribution of states as a function of energy and can also be used to measure the energy gap in semiconductors. In this work, our calculated TDOS in Figure 6 shows that the bulk CeO_2 is intrinsically an insulator (where E=0.0 eV represents the Fermi level in all TDOS figures). The highest occupied valence band exhibits significant O-2*p* states, while the narrow band situated just above the Fermi level is mainly due to the Ce 4 *f* states. The states situated above the empty Ce 4 *f* states are due to the 5*d* states. The calculated energy gaps are ~1.5 eV between O-2*p* and Ce-4 *f* states and ~ 5.7 eV between O-2*p* and Ce-5*d* states.

The TDOS was computed for all unreduced (111), (110) and (100) CeO_2 surfaces respectively as shown in Figure 6. We investigated the change in energy band gap between O-2*p* and Ce-4*f* states in all unreduced surfaces. The energy gap is smaller than that in the bulk by 0.1eV, 0.3eV and 0.25 eV respectively.

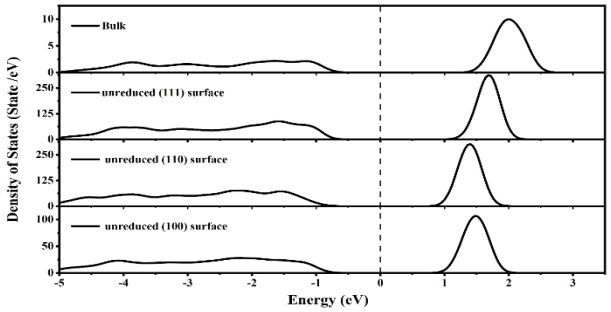

Fig. 6: Total density of state (TDOS) of bulk CeO_2, unreduced (111), (110) and (100) CeO_2 surfaces.

The TDOS of the reduced (111), (110) and (100) CeO_2 surfaces are shown in Figure 7. The reduced surfaces show that the Ce-4f state becomes partially filled and some new states appear in the middle of the gap between the Ce-4f and O-2*p* states as a result of removing oxygen. These new states in the DOS change the nature of ceria from insulator to a semiconductor in the case of (111) surface and to semi-metallic in the case of (110) and (100) ceria surfaces.

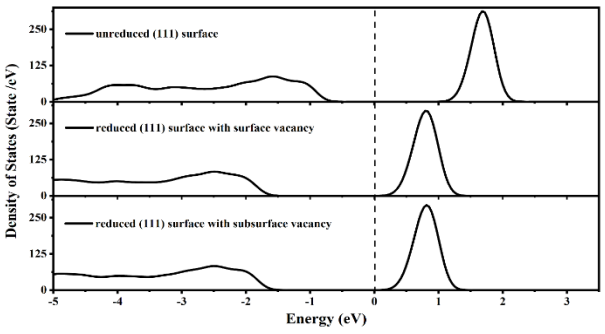

(a)

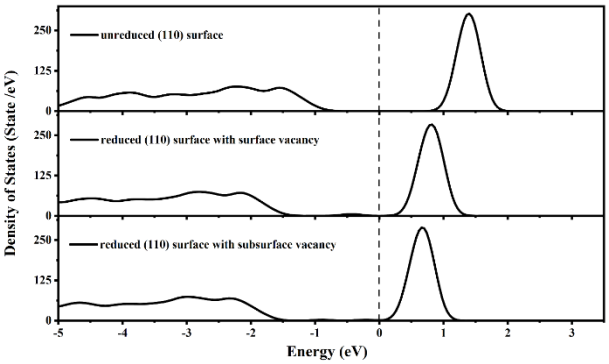

(b)

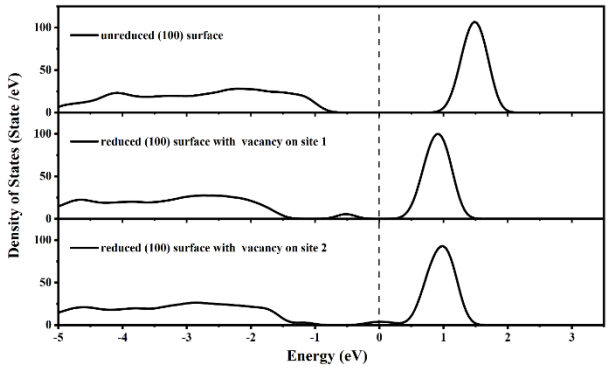

(c)

Fig. 7: TDOS for the unreduced and reduced (a) (111) CeO_2 surface (vacancy on surface and vacancy on subsurface), (110) CeO_2 surface (vacancy on surface and vacancy on subsurface), and (100) CeO_2 surface (vacancy on site 1 and vacancy on site 2)

4. Conclusion

We performed DFT study of the surface of reduced CeO_2 within LSDA+U approximation for three high symmetry surfaces, i.e. (111), (100), and (110). we studied the formation mechanism of oxygen vacancy sites on CeO_2 (111), (110), and (100) surfaces and their stability near the ceria surface regions. Both surface and subsurface oxygen vacancies induce the electron localization of reduced CeO_2 on all these three terminations of the surface, leading to the appearance of Ce^{3+} sites. The location of the Ce^{+3} following oxygen vacancy is found using Bader Charge Analysis (BCA). In the case of the CeO_2 (111) surface, oxygen vacancy at the surface and subsurface forms Ce^{3+} at next nearest neighbor to the vacancy. This is consistent with the experimental finding that the ratios of these two types of oxygen vacancy are nearly the same. In the case of CeO_2 (100) and (110) surfaces, Ce^{3+} is formed at the sites nearest to the oxygen vacancy sites. Experiments find that the reduced ceria catalyzes the dissociation of molecules on it surface. The dissociation is assisted by the oxidation of Ce^{3+} that is generated on reduced ceria surfaces. Our TDOS calculations show that the (111), (110) and (100) unreduced

ceria surfaces display differences in the band gap compared to that for bulk CeO_2. On the other hand, TDOS of the reduced surfaces shows that the Ce 4 *f* states are partially occupied and appeared in a new state near the band gap. It was revealed that the existence of these new states had a significant impact on the nature of ceria. The material is still a semiconductor with a smaller band gap on the surface of (111) ceria. The crossing of the new fermi level, which transforms ceria into a semi-metallic material, causes the surfaces of (110) and (100) ceria to become semi-metallic. As a result, it is anticipated that the development of oxygen vacancy will alter the conductivity and chemical characteristics of ceria.

Acknowledgments

The Authors would like to thank The Hashemite University for providing us with the support.

Conflict of Interests Statements

The authors of this article declare no conflict of interest.

References:

[1] H. YAO, Ceria in automotive exhaust catalysts I. Oxygen storage, *J Catal*., **86**, 254–265 (1984).

[2] L. Vivier, D. Duprez, Ceria-Based Solid Catalysts for Organic Chemistry, *ChemSusChem*., **3**, 654–678 (2010).

[3] A.Bueno-López, Diesel soot combustion ceria catalysts, *Appl Catal B*., **146**, 1–11(2014).

[4] K. Razmgar, M. Altarawneh, I. Oluwoye, G. Senanayake, Ceria-Based Catalysts for Selective Hydrogenation Reactions: A Critical Review, *Catalysis Surveys from Asia*., **25**, 27–47 (2021).

[5] A. M. Akondi, R. Trivedi, B. Sreedhar, M.L. Kantam, S. Bhargava, Cerium-containing MCM-41 catalyst for selective oxidative arene cross-dehydrogenative coupling reactions, *Catal Today*., **198**, 35–44 (2012).

[6] J. Qin, Y. Long, W. Wu, W. Zhang, Z. Gao, J. Ma, Amorphous Fe2O3 improved [O] transfer cycle of Ce4+/Ce3+ in CeO2 for atom economy synthesis of imines at low temperature, *J Catal.,* **371**, 161–174 (2019).

[7] D. Schweke, L. Shelly, R. Ben David, A. Danon, N. Kostirya, S. Hayun, Comprehensive Study of the Ceria–H $_2$ System: Effect of the Reaction Conditions on the Reduction Extent and Intermediates, The *Journal of Physical Chemistry C*., **124**, 6180–6187 (2020).

[8] S. Ackermann, L. Sauvin, R. Castiglioni, J.L.M. Rupp, J.R. Scheffe, A. Steinfeld, Kinetics of CO $_2$ Reduction over Nonstoichiometric Ceria, *The Journal of Physical Chemistry C.*, **119**, 16452–16461 (2015).

[9] F. Esch, S. Fabris, L. Zhou, T. Montini, C. Africh, P. Fornasiero, G. Comelli, R. Rosei, Electron Localization Determines Defect Formation on Ceria Substrates, *Science*, **309**, 752–755 (2005).

[10] S. Torbrügge, M. Reichling, A. Ishiyama, S. Morita, Ó. Custance, Evidence of Subsurface Oxygen Vacancy Ordering on Reduced, *Phys Rev Lett*., **99**, 056101 (2007).

[11] J.-F. Jerratsch, X. Shao, N. Nilius, H.-J. Freund, C. Popa, M.V. Ganduglia-Pirovano, A.M. Burow, J. Sauer, Electron Localization in Defective Ceria Films: A Study with Scanning-Tunneling Microscopy and Density-Functional Theory, *Phys Rev Lett.,* 106, 246801 (2011).

[12] M. V. Ganduglia-Pirovano, J.L.F. Da Silva, J. Sauer, Density-Functional Calculations of the Structure of Near-Surface Oxygen Vacancies and Electron Localization on CeO2(111), *Phys Rev Lett.*, **102**, 026101 (2009).

[13] G. E. Murgida, M.V. Ganduglia-Pirovano, Evidence for Subsurface Ordering of Oxygen Vacancies on the Reduced CeO2(111) Surface Using Density-Functional and Statistical Calculations, *Phys Rev Lett.,* **110**, 246101 (2013).

[14] X. Li, Z. Li, X. Yang, L. Jia, Y.Q. Fu, B. Chi, J. Pu, J. Li, First-principles study of the initial oxygen reduction reaction on stoichiometric and reduced CeO2 (111) surfaces as a cathode catalyst for lithium–oxygen batteries, *J Mater Chem A Mater*., **5**, 3320–3329 (2017).

[15] X.-P. Wu, X.-Q. Gong, Clustering of Oxygen Vacancies at CeO2(111): Critical Role of Hydroxyls, *Phys Rev Lett.,* **116**, 086102 (2016).

[16] J. Kullgren, M.J. Wolf, C.W.M. Castleton, P. Mitev, W.J. Briels, K. Hermansson, Oxygen Vacancies versus Fluorine at CeO2(111): A Case of Mistaken Identity?, *Phys Rev Lett.,* **112**, 56102 (2014).

[17] G. Kresse, J. Furthmüller, Efficient iterative schemes for *ab initio* total-energy calculations using a plane-wave basis set, *Phys Rev B*., **54**, 11169–11186 (1996).

[18] G. Kresse, J. Furthmüller, Efficiency of ab-initio total energy calculations for metals and semiconductors using a plane-wave basis set, *Comput Mater Sci*., **6**, 15–50 (1996).

[19] S. Deshpande, S. Patil, S.V. Kuchibhatla, S. Seal, Size dependency variation in lattice parameter and valency states in nanocrystalline cerium oxide, *Appl Phys Lett*., **87**, 133113 (2005).

[20] F. Zhang, P. Wang, J. Koberstein, S. Khalid, S.-W. Chan, Cerium oxidation state in ceria nanoparticles studied with X-ray photoelectron spectroscopy and absorption near edge spectroscopy, *Surf Sci.*, **563**, 74–

82 (2004).

[21] D. A. Andersson, S.I. Simak, B. Johansson, I.A. Abrikosov, N. V. Skorodumova, Modeling of CeO2 , Ce2O3 , and CeO2−x in the LDA + U formalism, *Phys Rev B*., **75**, 035109 (2007).

[22] C. Loschen, J. Carrasco, K.M. Neyman, F. Illas, First-principles LDA+U and GGA+U study of cerium oxides: Dependence on the effective U parameter, *Phys Rev B.,* **75**, 035115 (2007).

[23] S. Fabris, S. de Gironcoli, S. Baroni, G. Vicario, G. Balducci, Taming multiple valency with density functionals: A case study of defective ceria, *Phys Rev B.,* **71**, 041102 (2005).

[24] N. V. Skorodumova, R. Ahuja, S.I. Simak, I.A. Abrikosov, B. Johansson, B.I. Lundqvist, Electronic, bonding, and optical properties of CeO2 and Ce2O3 from first principles, *Phys Rev B.,* **64**, 115108 (2001).

[25] Y. Lin, Z. Wu, J. Wen, K.R. Poeppelmeier, L.D. Marks, Imaging the Atomic Surface Structures of CeO_2 Nanoparticles, *Nano Lett.*, **14**, 191–196 (2014).

[26] Y. Pan, N. Nilius, C. Stiehler, H.-J. Freund, J. Goniakowski, C. Noguera, Ceria Nanocrystals Exposing Wide (100) Facets: Structure and Polarity Compensation, *Adv Mater Interfaces*., **1**, 1400404 (2014).

[27] Z. Wu, M. Li, J. Howe, H.M. Meyer, S.H. Overbury, Probing Defect Sites on CeO_2 Nanocrystals with Well-Defined Surface Planes by Raman Spectroscopy and O_2 Adsorption, *Langmuir.,* **26**, 16595–16606 (2010).

[28] X. Wang, J.A. Rodriguez, J.C. Hanson, D. Gamarra, A. Martínez-Arias, M. Fernández-García, In Situ Studies of the Active Sites for the Water Gas Shift Reaction over Cu−CeO_2 Catalysts: Complex Interaction between Metallic Copper and Oxygen Vacancies of Ceria, *J Phys Chem B*., **110**, 428–434 (2006).

[29] X. Liu, K. Zhou, L. Wang, B. Wang, Y. Li, Oxygen Vacancy Clusters Promoting Reducibility and Activity of Ceria Nanorods, *J Am Chem Soc*., **131**, 3140–3141 (2009).

[30] Z. Yang, T.K. Woo, M. Baudin, K. Hermansson, Atomic and electronic structure of unreduced and reduced CeO2 surfaces: A first-principles study, *J Chem Phys.,* **120**, 7741–7749 (2004).

[31] M. Nolan, S. Grigoleit, D.C. Sayle, S.C. Parker, G.W. Watson, Density functional theory studies of the structure and electronic structure of pure and defective low index surfaces of ceria, *Surf Sci*., **576**, 217–229 (2005).

[32] H.-Y. Li, H.-F. Wang, X.-Q. Gong, Y.-L.Y. Guo, Y.-L.Y. Guo, G. Lu, P. Hu, Multiple configurations of the two excess 4f electrons on defective CeO2(111): Origin and implications, *Phys Rev B.*, **79**, 193401 (2009).

[33] M. Fronzi, S. Piccinin, B. Delley, E. Traversa, C. Stampfl, Water adsorption on the stoichiometric and reduced CeO2(111) surface: a first-principles investigation, *Physical Chemistry Chemical Physics*., **11**, 9188 (2009).

[34] J. J. Plata, A.M. Márquez, J.Fdez. Sanz, Electron Mobility via Polaron Hopping in Bulk Ceria: A First-Principles Study, *The Journal of Physical Chemistry C.*, **117**, 14502–14509 (2013).

[35] Y.-G. Wang, D. Mei, J. Li, R. Rousseau, DFT+U Study on the Localized Electronic States and Their Potential Role During H_2O Dissociation and CO Oxidation Processes on CeO_2 (111) Surface, *The Journal of Physical Chemistry C.*, **117**, 23082–23089 (2013).

[36] S. M. Kozlov, K.M. Neyman, O vacancies on steps on the CeO2(111) surface, *Physical Chemistry Chemical Physics*., **16**, 7823 (2014).